IJE TRANSACTIONS A: Basics Vol. 34, No. 10, (October 2021) 2319-2331

International Journal of Engineering

Journal Homepage: www.ije.ir

Seismic Analysis of Double Deck Floating Roofs of Siraf Storage Tanks with Condensate, Light and Heavy Crude Oils

H. Ahmadi*[a], M. H. Kadivar[b]

[a] *International College, Shiraz University, Shiraz, Iran*
[b] *School of Mechanical Engineering, Shiraz University, Shiraz, Iran*

PAPER INFO

Paper history:
Received 2 July 2021
Received in revised form 17 August 2021
Accepted 23 August 2021

Keywords:
Hydroelasticiy
Slosh
Foam Seal
Fluid-Structure Interaction
Earthquake

ABSTRACT

Seismic vibration of the double deck floating roof of Siraf storage tanks located in southern Iran has been studied. Condensate of Nar and Kagan gas field in the south of Iran as a very light hydrocarbon, Lavan as light and Soroosh as heavy crude oil content have been chosen. In addition to fluid-structure interaction, intermediate stiffeners, foam seal with nonlinear radial compression behavior and contact friction between the seal and the inner side of the wall are also considered. Under the above conditions, modal and time history analysis have been performed. For time history analysis, Sarpol-e Zahab and Shonbeh earthquakes in Zagros seismotectonic province of Iran and Sakaria as an earthquake near Iran were selected. Dominant natural frequencies, mode shapes of the roof parts and damping ratios of the first and second natural frequencies in addition to overall and spectral behavior of the roof in each liquid case were obtained and discussed. Changing condensate to Soroosh oil made about 17% hydroelastic natural frequency decrement and about 10% damping ratio decrease for the first natural frequency. The results showed that dominant natural frequencies and the relevant damping ratios decrease with moving from light to heavy liquid. The vibration of the roof fundamentally depends on the frequency content of earthquakes to such natural frequencies. Also, a floating roof in heavier liquid is more vulnerable to vibration according to the scaling method and steady-state amplitude.

***doi**: 10.5829/ije.2021.34.10a.13*

NOMENCLATURE

$[C]$	Proportional damping matrix	u_i	The steady-state amplitude of the i^{th} mode (m)
$[F]$	Excitation coefficient matrix	$\{W\}$	Modal displacement of the roof
g	Gravity (m/s^2)	**Greek Symbols**	
i	Natural frequency number	φ	Interpolation function
$[M]$	Modal mass matrix	ς	Damping ratio
$[K]$	Modal stiffness matrix	ρ	Density (kg/m^3)
$[R]$	Excitation participation matrix	ω_i	i^{th} natural frequency
$[S]$	Inertial coefficient matrix	**Subscripts**	
$[U]$	Stiffness coefficient matrix	r	Roof
u_g	Tank base displacement excitation (m)	add	Added mass or stiffness

1. INTRODUCTION

A floating roof is one of the ways to prevent product evaporation loss from storage tanks and to eliminate the possibility of a flammable atmosphere. The floating roof rises and falls with the liquid level to help reduce evaporation and prevent the buildup of dangerous gases. There are two geometrical types of floating roof: Single Deck Floating Roof (SDFR) and Double Deck Floating Roof (DDFR). SDFR consists of a deck plate and an

*Corresponding Author Institutional Email: a*hmadihs1354@gmail.com* (H. Ahmadi)

Please cite this article as: H. Ahmadi, M. H. Kadivar, Seismic Analysis of Double Deck Floating Roofs of Siraf Storage Tanks with Condensate, Light and Heavy Crude Oils, International Journal of Engineering, Transactions A: Basics, Vol. 34, No. 10, (2021) 2319-2331

outer pontoon. DDFR is fundamentally made up of lower deck, upper deck and stiffening structures between them. Figure 1 shows the schematic configuration of a DDFR storage tank. SDFR is normally used for relatively small and DDFR for larger tank diameter [1]. Due to the wider application of DDFR, this type has been considered for analysis. However, general conclusions can be extended to SDFRs.

Due to the extensive use of floating roofs throughout the industry to store volatile and flammable products such as crude oil or condensate, safety-related attention must be considered seriously. The liquid surface of the storage tank can undergo long period oscillations during seismic excitation which is called the sloshing phenomenon [2]. As sloshing is a liquid-surface phenomenon, floating roofs are more exposed to such oscillations. In addition, buoyancy consideration of the roofs makes them more vulnerable to instability. Hence, Floating roof oscillations due to slosh may result in devastating consequences such as the sinking of the roof, vast destructive fires and/or release of flammable or toxic products from the tank. For example, during the 2003 Tokachi-oki earthquake in northern Japan, seven storage tanks experiencing large amplitude slosh suffered severe damages such as ring fires and sinking of floating roofs. In one tank with a ring fire, the flame was confined to the rim of the tank roof. The sinking of the roof in another tank leads to open-top fire. Some other tanks also suffered sinking of the floating roof, exposing the kerosene to the atmosphere [3]. During the 1999 Izmit earthquake in Kocaeli of Turkey, some tanks in Turpas refinery have suffered excessive sloshing and their roof rubbing with the walls and then created instantly sparks igniting the liquid. The fire then spread to other crude oil tanks damaging 30 to 45 tanks covered by a floating roof [4]. Hence, seismic analysis of floating roofs is important. The several attempts which were made toward vibration mitigation of floating roof vibration and risk assessment of petroleum storage tanks indicate the importance of this field [5-8].

Numerous efforts were made to improve the structural and analytical model of a floating roof in seismic analysis. As an early attempt, Amabili [9] studied vibrations of circular plates resting on a sloshing liquid free surface. Golzar et al. [10, 11] idealized floating roofs as an isotropic elastic plate with uniform stiffness and thickness. Matsui [12] modeled SDFR as an elastic curved beam connected to the pontoon. Salarieh et al. [13] modeled deck plate as a flexural element rather than a membrane. Yamauchi et al. [14] discussed the nonlinearity of the SDFR deformation pattern. Sakai et al. [15, 16] assumed some uniform circumferential web plates at equal radial distances of the deck to model a more actual floating roof. Yoshida et al. [17, 18] introduced an axis-symmetric finite element model for the roof to obtain natural periods and vibration modes of the floating roof due to sloshing. Utsumi et al. [19] investigated internal resonances in the vibration analysis of the SDFR. Goudarzi [20] considered a contribution of the second sloshing mode to the seismic behavior of the SDFR. He considered some detailed geometry of the floating roof including compartments and inside truss works in the numerical model [21]. Meera and Reshmi [22] investigated the dynamic stability of SDFR with and without deck stiffeners. In the latter study, only modal analysis was performed.

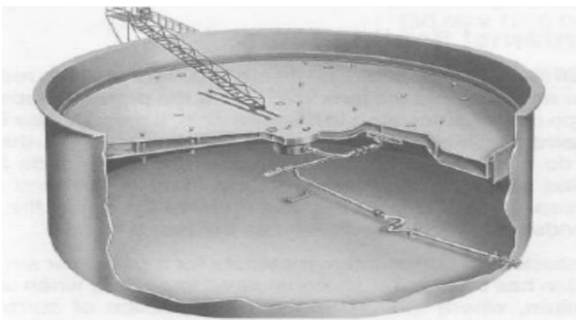

Figure 1. Schematic configuration of a DDFR storage tank [1]

To prevent product loss and atmospheric contamination, the gaps between the outer rim of the floating roof and the tank are closed up by flexible seals. There are scarce studies considering the outer rim seal in seismic analysis. Hosseini et al. [23] modeled the seal by introducing some radial pre-compressed only-compression springs for calculating the seismic response of the SDFR. Belostotsky et al. [24] addressed a non-linear radially located two-node element for the seal.

In our work, in addition to intermediate stiffeners, foam seal with nonlinear radial compression behavior and friction between the seal and the inner side of the wall are also considered.

Coupling of liquid slosh to the floating roof vibration is established through Fluid-Structure Interaction (FSI) [25]. Literature review about this phenomenon can help to find out the fundamental effects of liquid on floating roof vibration. In this regard, Sakai et al. [15] derived analytical relations for obtaining added mass and added stiffness matrix of liquid in the presence of a flexible floating roof. Shabani and Golzar [26] and also Sivy et al. [27] introduced the contribution of the fluid to the excitation value in addition to considering the added mass and added stiffness of the liquid. Shabani [28] introduced a complete contribution of the fluid by adding a damping matrix accounting for viscous liquid-wall interaction and friction between roof and wall. In the aforementioned works, each seismic analysis of floating roof was limited to a specified liquid content, and the vibration result cannot be demonstrated explicitly in terms of liquid properties. On the other hand, there are extensive types of petroleum products throughout oil industries having different densities and viscosities. In addition, ambient temperature variation can change these

properties. In the present study, numerical methods based on a finite element have been established for evaluating the effect of liquid variation on floating roof vibration. In this way, added mass, added stiffness and excitation effects are involved in the analysis. Rayleigh damping are also considered for structures and liquid. As a case study, seismic analysis of a DDFR including condensate, light and heavy Iranian crude oil has been performed. A storage tank located in Siraf port of Iran is selected for analysis, and is excited by significant earthquakes occurred in and near the country. Statistical analysis of Yazdani and Kowsari [29] predicted high probability density of earthquake occurrence for Zagros seismotectonic province. On the other hand, many of oil storage tanks of crude oil are situated in this seismotectonic province. Therefore, two earthquakes of this province are selected for analysis as domestic ground motion events.

2. FLOATING ROOF VIBRATION ANALYSIS

Assuming a simplified orthogonality condition, the hydroelastic behavior of the system is defined as [28]:

$$([M_r] + [M_{add}])\{\ddot{W}\} + [C]\{\dot{W}\} + ([K_r] + [K_{add}])\{W\} = -[R]\ddot{u}_g \quad (1)$$

In Equation (1), the contribution of the liquid to hydroelastic vibration of the roof is represented by added mass, added stiffness, proportional damping and excitation participation matrices. The uncoupled added mass matrix can be defined by:

$$[M_{add}] = \rho[S] \quad (2)$$

the added stiffness matrix by:

$$[K_{add}] = \rho g[U] \quad (3)$$

and excitation participation matrix by:

$$[R] = \rho[F] \quad (4)$$

Using Equation (1), the equation of motion for the i^{th} mode can be written as:

$$\ddot{w}_i(t) + 2\omega_i\varsigma_i\dot{w}_i(t) + \omega_i^2 w_i(t) = -\frac{\rho[F]}{[M_r]+\rho[S]}\ddot{u}_g(t) \quad (5)$$

Equation (5) summarizes the contribution of liquid in the form of natural frequency, light damping and excitation.

Application of u_g as a sinusoidal excitation and following the procedure represented by Chopra [30], the roof displacement at resonance varies with time as

$$w_i(t) = \frac{\rho[F]u_g}{[M_r]+\rho[S]}\frac{1}{2\varsigma}(1 - e^{-\varsigma\omega_n t})\cos\omega_n t \quad (6)$$

The seismic vulnerability of the system can be represented by steady-state vibration amplitude. The steady-state amplitude can be achieved by harmonic excitation of the base at natural frequency and computation of the amplitude after enough simulation time.

$$u_i = \frac{\rho[F]}{[M_r]+\rho[S]}\frac{u_g}{2\varsigma}\varphi \quad (7)$$

Equations (6) and (7) show that the effect of damping on the vibration response of the aforementioned system is also substantial.

3. ANALYSIS OF DOUBLE DECK STORAGE TANK

A cylindrical storage tank with DDFR that is under operation is considered for analysis. The General configuration of the main structural parts of the tank as illustrated in Figure 1. Modal and time history analysis have been performed to obtain the seismic behavior of the roof. In this regard, a finite element method using ANSYS Parametric Design Language (APDL) was employed, and a macro has been provided for hydroelastic analysis of the tank [31]. Figure 2 outlines the elemental model of the system. Cutaway views are used to permit the demonstration of all the essential parts in the figure.

The tank body and DDFR specifications are selected according to the Siraf storage tank located in the south of Iran. Specifications of the storage tank and shell are summarized in Table 1.

For liquid content, condensate of Nar and Kangan gas field in the south of Iran was selected as a very light hydrocarbon. In addition, Lavan was considered as light and Soroosh as heavy crude oil. Table 2 shows the density and viscosity of the three liquid types [32]. 8-node compressible fluid element has been selected for liquid analysis to calculate either the propagation properties of the waves in the environment and also Fluid-Structure Interaction (FSI). A pressure-based wave equation was utilized for numerical analysis of the fluid. In addition, for liquid-roof and liquid-shell interfaces, displacements DOF were also activated to establish FSI.

Another approach is the displacement-based wave equation. However, in this method, displacement Degrees Of Freedom (DOF) within the fluid may lead to zero pivots and divergence.

Floating roof dimensions are given in Table 3. Lower and upper decks of the roof are stiffened by bulkheads, trusses and rafters. In Figure 3, the overall configuration of the stiffeners has been demonstrated. Details of trusses and rafters are also shown in Figure 4. Bulkheads are dividing walls between separate compartments. 4-node shell elements with 6-DOF at each node were used for the lower deck, upper deck, bulkheads, and also for the shell body of the tank. Trusses have been modeled as 2-node beams to cover both translational and rotational DOF. 2-node beams were also used for rafter modeling.

There are various types of seals to fill the gap between the outer rim of the roof and shell such as pantograph, foam and tube seals. In this regard, foam seal as in Figure 5 has been selected. Floating roof seals are similar to gaskets as they fill the space between two mating surfaces for fluid leakage prevention. Thus, an 8-node gasket element with 3-DOF at each node has been chosen for seal modeling. The element is capable of both through-thickness and transverse shear deformation. Figure 6 shows a magnified picture in which the situation of the seal concerning the shell and stiffeners is depicted. Also, the nonlinear relation between radial stress and strain of the seal is shown in Figure 7. The governing stress-strain relationship has been estimated considering the reasonable stiffness of the foams provided by manufacturers [33]. This relation was entered into the macro via data tables. In ANSYS APDL, tabular data of material properties are activated using the TB command [31]. Elastic contributions of the seal accessories like seal envelopes are also considered in the stress-strain curve. In addition, an estimated value for the elastic behavior of the weather shield depicted in Figure 5 has been added to the peripheral constraint. The latter is sometimes referred to as a secondary seal with respect to the primary seal.

TABLE 1. Storage tank general and shell specifications

Parameter	Value
Tank height	14 m
Tank diameter	60 m
Rated wall thickness	0.02 m
Liquid height considering sufficient freeboard	12 m
Metal density	7850 kg/m3
Metal Young's modulus (Low carbon steel)	2e11 N/m2
Metal Poisson's ratio	0.3
Metal damping ratio	0.03

TABLE 2. Specifications of three liquid content cases

Liquid type	Density (kg/m^3)	Viscosity (10^{-3} Pa.s)
Natural gas condensate	648	0.89
Lavan (Light crude oil)	848	6.16
Soroosh (Heavy crude oil)	941	698.64

TABLE 3. Floating roof dimension

Parameter	Value (m)
Height	0.672
Upper deck thickness	0.00477
Lower deck thickness	0.00637
Height in contact with seal	0.40
Gap between roof rim and shell	0.20

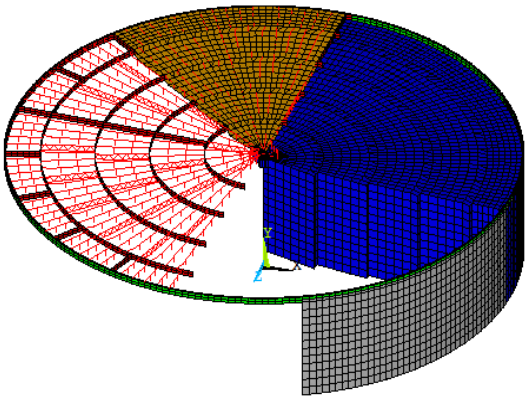

Figure 2. Cutaway views of the overall model (blue: liquid, brown: upper deck, red: roof stiffeners, green: seal, grey: shell)

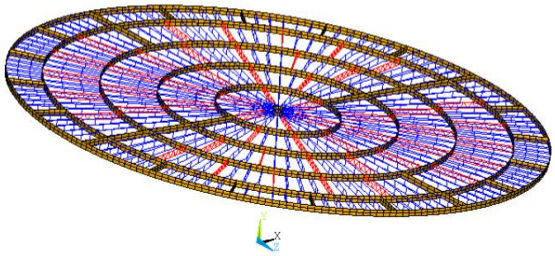

Figure 3. Eelemental configuration of the intermediate stiffeners of the roof (red: trusses, blue: rafters, brown: bulkheads)

Figure 4. Detail of trusses and rafters of the roof

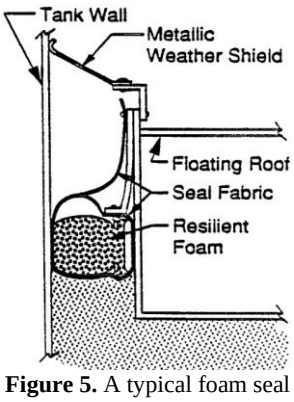

Figure 5. A typical foam seal

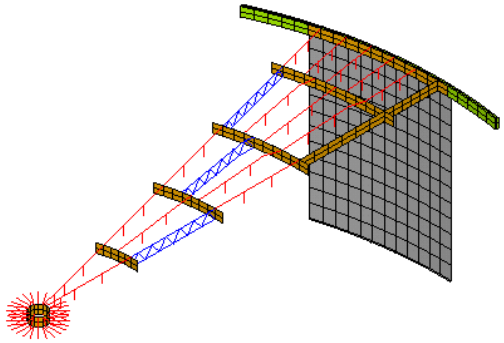

Figure 6. Magnified picture of shell(grey), seal(green), bulkheads(brown), rafters(red) and trusses(blue)

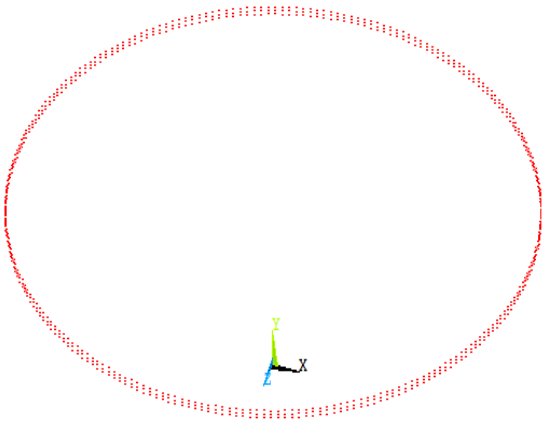

Figure 8. Distribution of contact elements around the seal

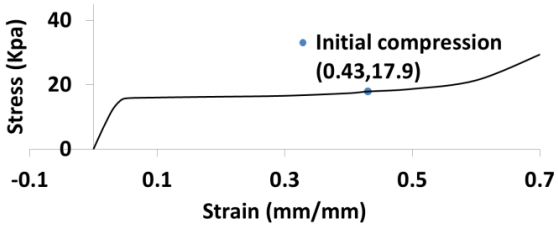

Figure 7. Stress-strain diagram of foam seal with Initial Stress and Strain

The roof seal is installed by an initial compression. The initial compressive stress of 17.9KPa has been considered for sealing. Having the stress value, the initial compressive strains can be obtained from Figure 7 as

$$\varepsilon_0 = 0.43 mm / mm. \quad (8)$$

The outer rim of the floating roof is in contact with the inner side of the shell. Thus, the boundary conditions of the roof are different from almost most studies performed in the literature. Seals are fixed to the outer rim of the floating roof to have vertical movement with it during liquid level variation. However, the seal and shell movements are different. Thus, friction forces between the seal cover and shell are considered in this work. Contact force transmission will be established only in the case of closed contact [31]. Several approaches are available for defining contact interaction between the inner side of the shell and seal. In this study, node-to-node contact elements have been chosen. The distribution of contact elements between the seal and shell has been shown in Figure 8. This type of element represents contact and sliding between any two nodes of the shell and seal. The element has two nodes with three translational DOF at each node. It is capable of supporting compression in the normal direction of contact and Coulomb friction in the tangential direction. Weak springs with 1e-6N/m stiffness have been taken into account to prevent open contact and to aid in convergence, but sliding is permitted throughout the analysis. Solution of contact force and displacement is performed by contact algorithm. Several contact algorithms are available for the solution of contact problems such as Lagrange multiplier and penalty method. By the penalty method, tangential stiffness can be obtained by multiplication of friction coefficient and radial stiffness, which is suitable for the current study. Therefore, the penalty method has been selected.

For damping consideration, light damping has been adopted for the overall system. For structural parts, the metal damping ratio as in Table 1 was used. For liquid, viscous dissipation of the surface waves according to Table 2 was considered as the primary source of liquid damping. Damping of the seal was estimated according to the usual hysteresis loops present in polyurethane (PU) foams [34]. The equivalent damping ratio due to contact friction was approximately calculated based on friction coefficient between nylon and steel (0.6), average radial stress (from Figure 7), contact area and average critical damping (computed from the result of modal analysis). For the equivalent damping ratio calculation method readers can refer to [35].

The tanks are assumed to be anchored to the rigid ground such that no sliding or uplift may occur. Therefore, all base nodes located on the floor are fully restrained in all directions. As a result of this perfect anchorage assumption, the tank floor may not be included in the FE modeling of such containers. Since only an anchored tank is considered in this study, the tank floor is not modeled in FE simulation [36].

Gravity acceleration (g) has been applied to the liquid as body acceleration. Initial hydrostatic stability was established by ignoring the gravity acceleration of the roof. Hence, pressure results on the roof-liquid interface will be dynamic pressure, i.e. pressure due to the roof oscillation in the fluid.

FSI was applied for both shell-liquid and roof-liquid interfaces by the selection of liquid and structure nodes

and elements at the interface. Then, the surface load at the selected nodes was labeled as FSI. Common nodes have been used for fluid and structure elements at the shell. However, for the roof lower deck and liquid surface, different nodes have been used but with the same vertical and radial position.

Modal and time history analysis have been performed considering the aforementioned models. Modal analysis was implemented by a solution to the eigenvalue problem. For time history solution with the FSI problem, simultaneous or partitioned coupling can be employed. In simultaneous strategy, the whole system is treated as a monolithic entity, and the components are advanced simultaneously in time. In partitioned treatment, the field models are treated computationally as isolated systems that are separately stepped in time. In this study, the simultaneous coupling method has been used for time history analysis [37]. For full transient Analysis, an optimized strategy has been taken considering time intervals, element sizes, the total number of elements and elements with contact algorithm. In this way, 0.03s time steps have been taken into account regarding 95071 elements and also so many node-to-node contact elements generated.

The linear solution assumes small deflection so that the resulting stiffness and mass distribution changes can be considered insignificant. In contrast, when a structure experiences large deflections, forces will change direction, and the elements will undergo large rotations and displacements. This effect is known as geometric nonlinearity which may substantially change the final results of a numerical analysis [21]. For such nonlinear analysis, Newmark's integration scheme solution was conducted in association with Newton-Raphson iterative algorithm [38]. After each time step, mass and stiffness matrices were updated to consider the geometric nonlinearity of the system.

4. RESULTS

Modal analysis was initially performed to obtain dominant frequencies. As stated before, FSI between fluid-Wall and Fluid-Roof has been considered. In Figure 2, the elemental configuration of the tank, liquid and roof was outlined. A total of 95071 elements have been generated in the system.

4. 1. Natural Frequencies The first dominant natural frequencies of the tank for different oil contents, i.e., Iranian condensate, Lavan and Soroosh crude oil are calculated and are shown in Table 4. The first two dominant natural frequencies are indexed as fn1 and fn2 for simplicity.

As it can be seen, the two fundamental natural frequencies for heavy crude oil i.e. Soroosh oil are about 17% less than for Iranian condensate, while this value for Lavan crude oil is about 5% less than for condensate.

4. 2. Mode Shapes The mode shape of the upper deck for the first two modes is shown in Figures 9 and 11. In addition, a sector of the deck has been selected and in this sector, the behavior of the upper, lower and intermediate structures including rafters, bulkheads and trusses are demonstrated (Figures 10 and 12).

As was shown in Figures 10 and 12, each element of the intermediate structure has its mode of vibration that affects and makes the final mode shape of the deck. Due to the continuity of the deck, in general, upper, lower and intermediate structures follow the same shape pattern. The bottom surface of the lower deck is in contact with the oil and its upper surface is connected to stiffeners. In addition, the lower deck is about 33% thicker than the upper deck. Hence, its amplitude is 2%~3% less than the upper deck. Maximum vibration will occur due to fn1 which is the most dominant natural frequency. Hereafter, the maximum absolute value of mode shapes will be referred to as the high spot that is the peak area of the upper deck as depicted in Figures 9 to 12.

As the main dynamic effect on the floating roof is due to the fluid sloshing, only vertical deformations (Y global direction) are shown. Inspection of the roof horizontal movements concerning the wall inside indicates relatively less value due to the nature of surface vertical waves.

As was expected, the modal shapes of the roof in all the three liquid contents, i.e. condensate, Lavan and Soroosh crude oils are almost the same as it is shown in Figures 10 and 12.

Detail of bulkheads, trusses and rafters for fn1 mode shape in and around high spot is depicted in Figure 13. This figure shows that rafters are more vulnerable to vibration than other stiffeners. This fact notifies the revision of the design regarding this structure.

As modal analysis is performed in the absence of excitation, and excitation is affected by liquid, the modal

TABLE 4. Natural frequencies of three liquid content cases

Liquid type	fn1 frequency (Hz)	fn2 frequency (Hz)
condensate	0.1813	0.7100
Lavan	0.1581	0.6236
Soroosh	0.1504	0.5920

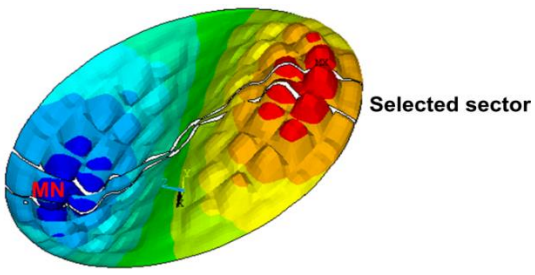

Figure 9. fn1 mode shape of the upper deck

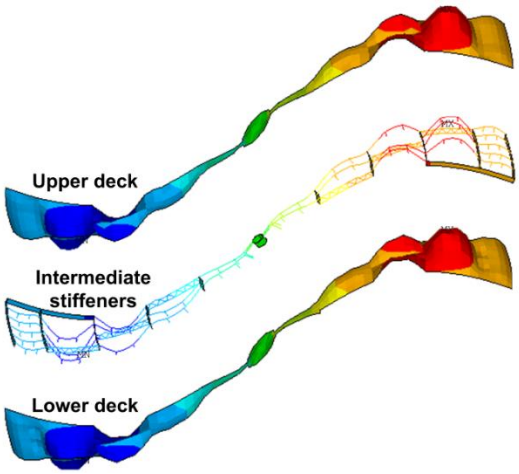

Figure 10. fn1 mode shape of the sector selected in Figure 8 including a lower deck, Intermediate structures and upper deck

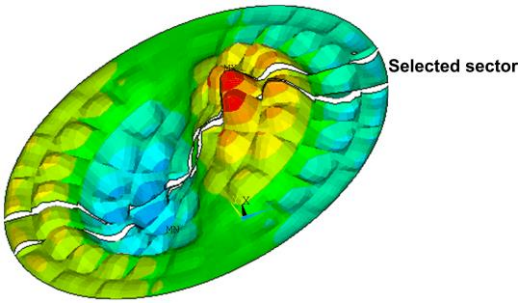

Figure 11. fn2 mode shape of the upper deck

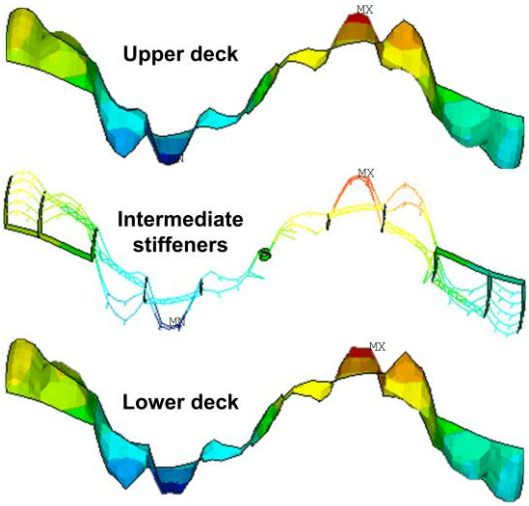

Figure 12. fn2 mode shape of the sector selected in Figure 10 including a lower deck, intermediate structures and upper deck

approach cannot represent the complete effects of the liquid on the vibration behavior of the roof according to Equation (1). Furthermore, vibration amplitude cannot be

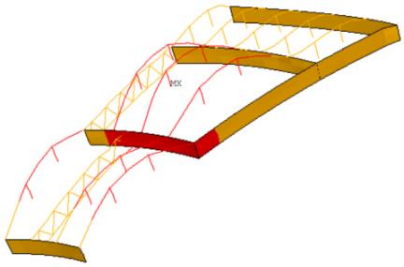

Figure 13. Mode shape detail of bulkheads, trusses and rafters for fn1

obtained by a modal approach. On the other hand, the vibration amplitude of the roof during an earthquake is the main concern in seismic analysis. One of the methods for amplitude evaluation of the vibrating systems is response spectrum modal analysis. This method was used so far for some structures [39] and open storage tanks [27]. However, this approach is based on linear theory, and accurate results cannot be achieved in this analysis. Hence, a more extensive effect of liquid properties variation on seismic behavior of the roof will be investigated in the next sections by performing time history analysis.

4. 3. Time History Analysis Time history analysis of the system has been performed during base acceleration excitation. The system specifications are as stated before and FSI is adopted as in the modal analysis. Nonlinear stress/strain relation of the seal and frictional contact were also used.

The base of the storage tank was excited horizontally by the 1999 Izmit earthquake in Sakaria of Turkey taken from SiesmoSignal software accelerograms [40], the 2017 Sarpol-e Zahab earthquake in the east of Iran [41] and the 2013 Shonbeh earthquake in the south of Iran [41]. The first two earthquakes have dominant amplitude at lower frequencies around fn1. Therefore, it has been employed for fn1 vibration evaluation. The two earthquakes have different properties at fn1 as will be shown in Figures 19 and 22. Excitation of Sarpol-e Zahab at fn1 increases from light to heavy oil. Sakaria acts in the reverse order; it decreases from light to heavy oil at fn1. More detail of the figures will be described in advance. The motivation of the choice is to see how much difference can affect DDFR response at fn1. Regarding the aforementioned characteristic, earthquakes such as El Centro which have critical point near fn1 in amplitude vs frequency function are not suitable for this purpose.

Shonbeh earthquake has dominant vibration at higher frequencies. Hence, it was used for fn2 excitation. However, some frequency modulations were applied to the strong portion of it to be more effective on fn2.

All the prescribed vibration modes were observed in the time history analysis. El Centro earthquake was employed as a rich frequency content earthquake for

producing a combination of several modes together. For instance, Figure 14a shows the simultaneous appearance of fn1 and fn2 modes of the upper deck for Soroosh oil content at t=8.67s excited by this earthquake. In Figure 14b, a mode shape obtained by Meera and Reshmi [22] for a DDFR with a fixed boundary has been illustrated. Comparison of the periphery displacement of the two mode shapes verifies the involvement of friction around the roof periphery in the present work.

In Figure 15, the vibration pattern of different parts of the tank due to the Sakaria earthquake was shown in cutaway views. In addition, dynamic pressure on the liquid surface at the same time was demonstrated in Figure 16. As can be observed, the pressure profile on the contact area satisfies the displacement profile of the roof, i.e. maximum liquid dynamic pressure on the roof coincides with maximum displacement, and minimum pressure coincides with minimum displacement. This phenomenon verifies FSI existence at the roof-oil interface. In each figure, maximum and minimum spots are denoted by 'MX' and 'MN' respectively.

Vibration amplitude has been investigated in time and frequency domains. In this way, the high spot vibration of the upper deck has been selected for time wave demonstration. This spot was indicated in Figure 9 as MN in red color.

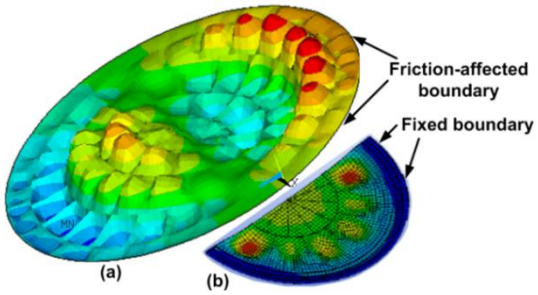

Figure 14. (a) Vibration pattern of the upper deck at t=8.67s for Soroosh crude oil content due to El Centro earthquake, (b) mode shape obtained by Meera and Reshmi [22]

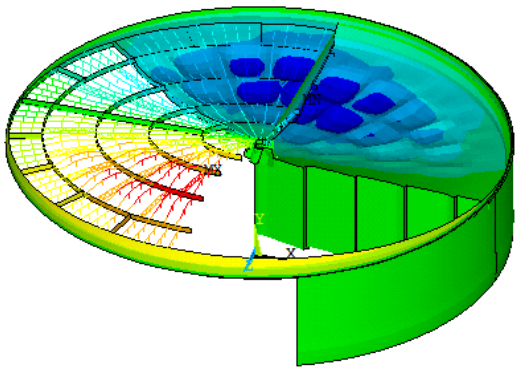

Figure 15. Vertical vibration pattern of the different parts of the tank in cutaway views due to Sakaria earthquake at t=7.29s

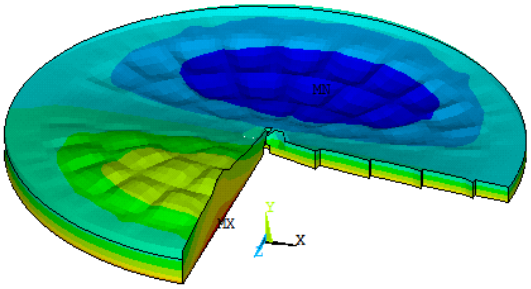

Figure 16. Pressure pattern of the oil surface due to Sakaria earthquake at t=7.29s (Minimum pressure is indicated by MN and maximum by MX)

In Figure 17, the time history of the Sarpol-e Zahab earthquakes has been demonstrated. In the current study, Peak Ground Acceleration (PGA) has been taken 0.3g as can be observed in the excitation time waves. Figure 18 gives vibration amplitudes of the roof for the three liquid content cases in the time domain due to this ground excitation. The earthquake duration was the 30s. However, time history analysis was extended up to the 40s to have forced and some free vibration. As it can be seen, DDFR vibration's amplitude increases from condensate to Soroosh crude oil during the Sarpol-e Zahab earthquake. Also, as is expected, the heavier oil's amplitudes occur later than lighter oil due to its long period of time.

Figure 19 shows the Power Spectrum (PS) of the Sarpol-e Zahab earthquake and the roof's highest spot vibration due to this earthquake. As shown in the figure, dominant PS frequencies deviate a little from natural frequencies (solid circles) towards higher excitation. This phenomenon implies the influence of forcing frequency on PS in addition to the natural frequency.

In Figure 19, excitation has been increased from condensate to Soroosh oil for fn1. This manner causes the roof Root Mean Square (RMS) of vibration to increase from condensate to Soroosh crude oil.

The same method was used for fn2 vibration amplitude analysis. In this regard, the Shonbeh earthquake was found to have high-frequency contents, and therefore it was used for producing fn2 mode. However, frequency characteristics of the earthquake have been modified in each liquid case to have sufficient excitation values at fn2. In this excitation case, excitation amplitude and PS, and the resulting vibration magnitude and PS at fn2 have been increased from condensate to Soroosh crude oil.

In Figure 18 and also Shonbeh earthquake, vibration magnitude has been represented as a function of time. However, the liquid cases must be compared irrespective of time. Time parameters can be canceled out by extending simulation duration to infinity. For this purpose, the Sakaria earthquake was employed. The time history of this earthquake was shown in Figure 20. Figure 21 shows time domain vibration of the roof's highest spot

due to the Sakaria earthquake for more than 40s. Excitation was the 20s. However, an investigation was extended to the 120s as relative infinite time. Figure 22 gives PS relating to infinite time waves. In this figure, excitation and vibration amplitude RMS at fn1 have been decreased from condensate to Soroosh.

As it was seen, excitation at the natural frequency plays the main role in the amplitude decrement or increment. Roof vibration increases with excitation rise and vice versa. Hence, evaluation has been performed so far according to the frequency content of the excitation.

To have excitation-independent in addition to time-independent evaluation, the excitation curve in Figure 22 was scaled up so that it passes through the maximum PS of the condensate case. As can be seen, the positions of PS peaks for Lavan and Soroosh are slightly higher than the scaled excitation curve. This circumstance shows that a floating roof is more vulnerable to vibration in heavier liquids i.e. Lavan and Soroosh.

In another point of view, in the time wave demonstrations, sharp edges of the vibration curves imply high-frequency existence. Therefore, Figures 18 and 21 indicate that high-frequency vibrations generally decay faster than low-frequency ones due to more damping as can be expected. However, the time of disappearance also depends on the excitation initiation time. Hence, high-frequency components may have low

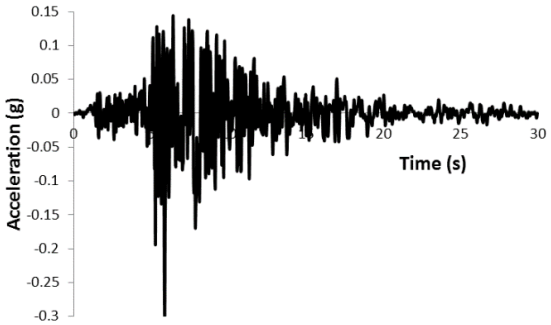

Figure 17. Time history of Sarpol-e Zahab earthquake

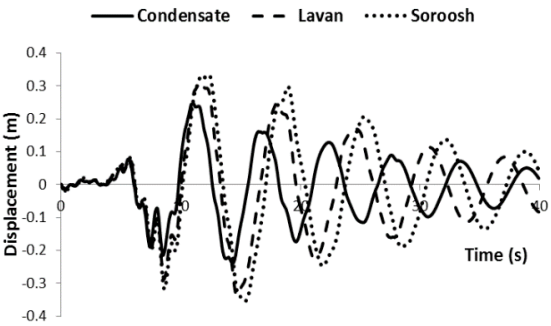

Figure 18. Time domain vibration of the roof highest spot for three liquid cases excited by Sarpol-e Zahab earthquake

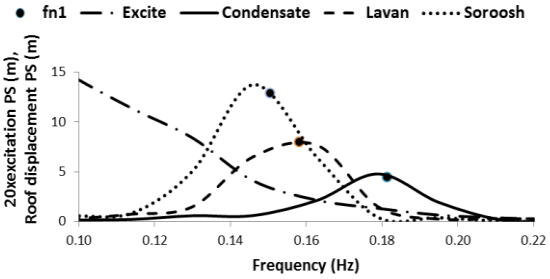

Figure 19. Vibration PS of Sarpol-e Zahab earthquake and the relevant roof highest spot for three liquid cases

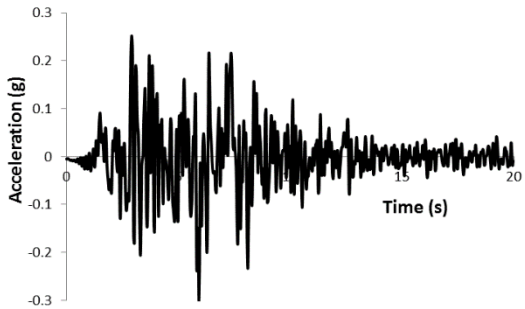

Figure 20. Time history of Sakaria earthquake

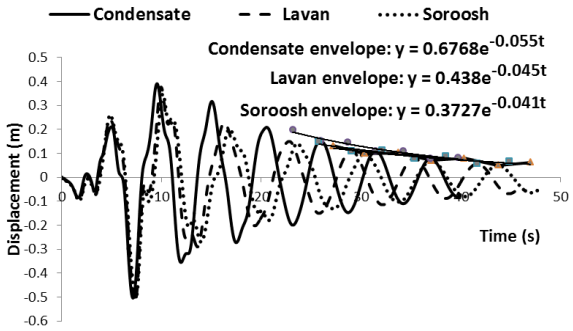

Figure 21. Time domain vibration of the roof highest spot for three liquid cases excited by Sakaria earthquake

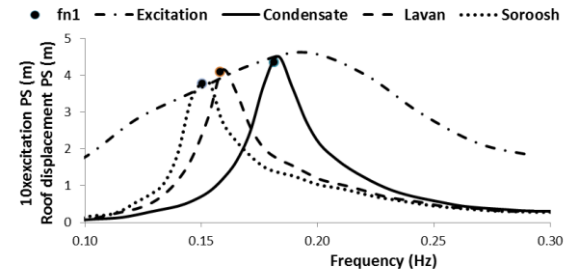

Figure 22. Vibration PS of Sakaria earthquake and the relevant roof highest spot for three liquid cases

or high contributions to the maximum vibration peak. For Sarpol-e Zahab earthquake as shown in Figure 18, maximum absolute displacement has been taken place after higher frequencies disappeared. On the other hand, in vibration due to the Sakaria earthquake, a trace of the second mode (fn2) exists in addition to the first mode (fn1). The influence of fn2 on the maximum peak can be recognized by comparing the high spot position of Figure 15 with Figure 9 corresponding to fn1 mode shape and Figure 11corresponding to fn2 mode shape. As can be seen, the high spot has moved slightly to the inside of the deck. After maximum peak elapses, fn2 will vanish earlier than fn1 so that the final cycles are approximately coincident with the fn1 time wave. This characteristic will be employed for the computation of the fn1 equivalent damping ratio.

The equivalent damping ratio is another factor that affects vibration response. In Figures 18 and 21, vibration decays more slowly in the last periods of free vibration expressing logarithmic decrement. Also, it was observed that natural periods obtained in the last periods of free vibrations conform to the natural periods determined by modal analysis. Hence, natural periods are approximately constant during simulation. Therefore, logarithmic decrement can be used for damping ratio determination during free vibration. Free vibration behavior after the Sakaria earthquake was employed for fn1 damping ratio computation. In this regard, the envelope curves and the relevant exponential relationships for the computation of fn1 equivalent damping ratios can be observed in Figure 21. For each liquid case, the exponent of the envelope curves in the free vibration part is '$-\varsigma\omega_1 t$'. Hence damping ratio can be computed for each case. The same method was employed for the calculation of the fn2 equivalent damping ratio. As stated before, the Shonbeh earthquake was used for producing vibration with fn2 dominant amplitude. Equivalent damping ratios of fn1 and fn2 obtained by this method have been summarized in Table 5. Tables 4 and 5 indicate that natural frequency values and damping ratios have been decreased from light to heavy liquid content. Damping decrement due to liquid variation is small for fn1. For instance, liquid change from condensate to Soroosh leads to a 10% decrement of damping ratio, while this value is 4% for Lavan to Soroosh. However, for fn2, natural frequencies and damping ratios are both affected substantially by liquid change. Hence, the system with heavier liquid has a smaller damping ratio. This phenomenon is because the heavier liquid has more participation in the roof vibration. As liquid has lower damping than that of structures, this phenomenon causes the damping ratio of the whole system to be decreased.

Stress evaluation of the floating roof has been performed by checking the stress of the upper and lower deck at the time of maximum displacement. This circumstance arose at 7.29s due to the Sakaria earthquake

TABLE 5. Equivalent damping ratios (ς) of the first and second natural frequencies for three liquid cases

Liquid type	ς for fn1	ς for fn2
condensate	0.0483	0.0646
Lavan	0.0453	0.0569
Soroosh	0.0434	0.0538

in the condensate case as can be observed in Figure 23. The upper deck undergoes more stress. Hence, the stress distribution of the upper deck in the earthquake direction was selected for demonstration and was shown in Figure 23. As can be seen, stress values are in the elastic limit of the roof material which is low carbon steel.

Von Mises stress of the upper and lower deck was also checked which exhibits safety of the structure according to maximum distortion energy criteria.

In this analysis, earthquakes were scaled to the peak ground acceleration of 0.3g to obtain convergent numerical conditions as possible. This scaling maintains main structural deformations in almost linear behavior. However, in hazardous conditions, excitation may exceed this value, and nonlinear behavior of the structure material is needed to be defined through data tables as described for foam seal material. On the other hand, large permanent deformations of the roof especially in the periphery may cause liquid splash or spill out which is a potential for roof instability or sinking. However, this process cannot be simulated by hydroelastic analysis which has been presented so far. Therefore, a low value of scaling is preferred.

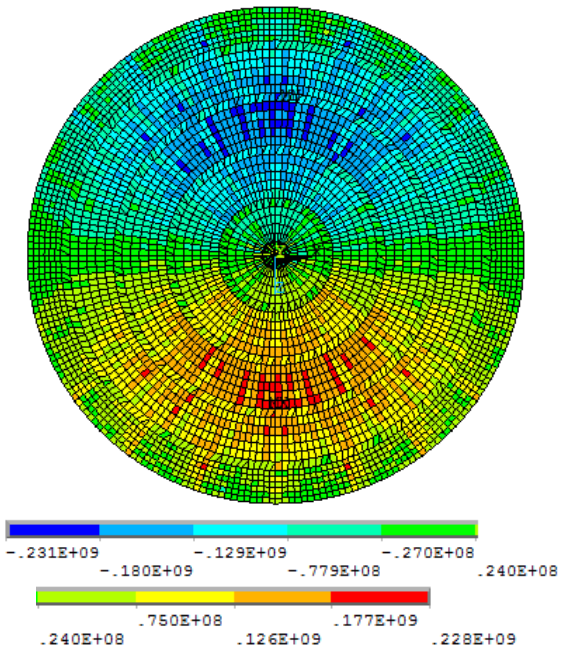

Figure 23. Stress distribution of the upper deck in the excitation direction at 7.29s during the Sakaria earthquake

The scaling method used in Figure 22 assumes a linear relationship between excitation and vibration amplitude. To add nonlinearity, the steady-state method has been proposed as an alternative. The basic concept of this procedure has been introduced in Equation (7). In this approach, the steady-state response of the roof in light and heavy crude oils is compared by applying equal harmonic amplitudes at their natural frequencies. Following this procedure, harmonic displacements at the first natural frequencies with equal amplitude were applied to the condensate tank as light and Soroosh as a heavy crude oil system as:

$$u_g = \begin{cases} 0.15\sin(1.1391t) & \text{(m) for condensate} \\ 0.15\sin(0.9450t) & \text{(m) for Soroosh} \end{cases} \quad (9)$$

Vibration responses were compared as shown in Figure 24. Simulation time was extended to steady-state condition to have time-independent evaluation. Refer to Equation (6) for more clarity. According to steady-state amplitude, a floating roof in heavy crude oil is more vulnerable to vibration than in lighter oil. It can be seen from Figure 24 that the heavier oil's steady-state amplitude occurs later than lighter oil due to its long period. These two phenomena conform to the results achieved in the previous analysis.

Figure 24 also shows that baseline of the oscillation is slightly lower than zero due to buoyancy problems.

5. VALIDATION OF NUMERICAL MODEL

The differences between the current numerical model with those available in the literature prevent us from achieving comparable models; Contact friction between seal and wall and the proposed complicated stiffeners haven't been presented so far. Also, the exact time wave and frequency characteristics of the excitation sources used in the literature are not accessible. Therefore, simplification of the proposed model is inevitable invalidation. In this regard, natural frequencies in the condition of the unroofed rigid tank were computed using the analytical technique recommended in European standard Eurocode 8 [42]. The considered tank was assumed to have fixed conditions at the base as in the present work. Characteristics of the model were then developed toward the current model in steps to investigate the result deviation. In the second step, the side shell was revised from rigid to flexible. This modification led to considerable change in a result that verifies FSI existence between shell and liquid. Afterward, a floating roof and seal were added to the model but without slipping permission for the roof along with the tank height. In this step, FSI between roof and liquid can be recognized from natural frequency change. Also, it can be verified further by investigation of Figures 15 and 16 as stated before. Finally, the model was completed by introducing a frictional slip between seal and shell. The contribution of slippage to the roof vibration has been verified in Figure 25. In this figure, the vibration time waveform of the same node at the roof periphery due to the Sakaria earthquake was compared for the two cases of no-slip and frictional slip. As can be seen, the maximum amplitude has been increased in frictional slipping cases. In addition, in Figures 14a and 14b, the frictional slipping boundary was compared with the fixed boundary. However, dominant natural frequencies have not been changed considerably by frictional slip addition in the actual range of friction coefficients. The result of the aforementioned gradual development of the model has been summarized in Table 6. The table also shows the substantial effect of the roof on fn2 frequency. Therefore, fn2 frequency is more structure-dependent than fn1.

So far, verification has been performed assuming zero dampings for the system. For further verification, the damping ratios provided in Table 5 were compared with Eurocode 8 recommendations that show acceptable agreement [42].

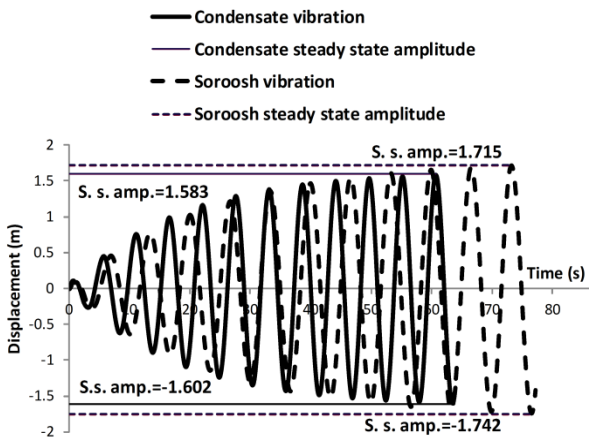

Figure 24. Vibration increment and steady-state amplitude of the roof for condensate and Soroosh crude oil in response to equal harmonic excitations

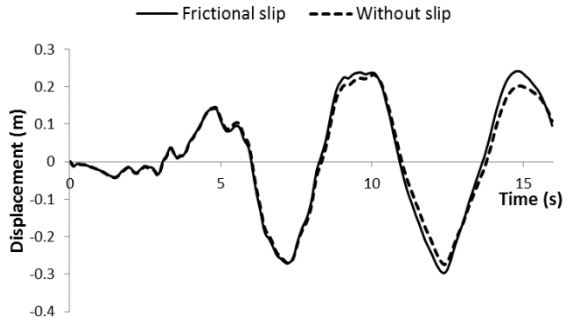

Figure 25. Maximum roof periphery vibration in no-slip and frictional slip cases of the seal-shell contact area

TABLE 6. The first and second natural frequencies for condensate liquid case with the gradual development of the model

Model type	fn1	fn2
Eurocode 8 for unroofed rigid tank	0.0978	0.2072
Current numerical model for unroofed rigid tank	0.0983	0.2081
Current numerical model for unroofed flexible tank	0.1345	0.2243
Current numerical model for a roofed flexible tank with seal and contact friction	0.1813	0.7100

6. CONCLUSION

The behavior of Siraf double deck floating roof, in the south of I.R.Iran, with foam seal and fluid-structure interaction were studied for condensate, light and heavy crude oils. It was seen that the upper, lower and intermediate structures have the same dominant mode shapes and it is important to keep this integrity in the design phase. The mode shape was almost independent of the oil's type. The natural frequency and damping ratio decrease as the oil becomes heavier. The first hydroelastic natural frequency of the roof in Soroosh oil, heavy oil, is about 17% less than for Iranian condensate, light oil while damping ratio decrease is about 10%.

The vibration of the roof mainly depends on the frequency content of the earthquake to the roof's hydroelastic natural frequencies. For Sarpol-e Zahab and Shonbeh earthquakes, the heavier oil had dominant amplitude while for the Sakari earthquake the lighter oil had dominant amplitude.

Floating roof in heavy crude oil is more vulnerable to vibration than in light oil according to scaling method and steady-state amplitude.

7. REFERENCES

1. Kuan, S.Y., "Design, construction and operation of the floating roof tank", University of Southern Queensland, Mechanical and Mechatronic Engineering, Australia, Bachelor of Engineering, (2009).
2. Trimulyono, A., Chrismianto, D., Samuel, S. and Aslami, M.H., "Single-phase and two-phase smoothed particle hydrodynamics for sloshing in the low filling ratio of the prismatic tank", ***International Journal of Engineering, Transactions B: Applications***, Vol. 34, No. 5, (2021), 1345-1351., DOI: 10.5829/IJE.2021.34.05B.30
3. Hatayama, K., "Lessons from the 2003 tokachi-oki, japan, earthquake for prediction of long-period strong ground motions and sloshing damage to oil storage tanks", ***Journal of Seismology***, Vol. 12, No. 2, (2008), 255-263., DOI: 10.1007/s10950-007-9066-y
4. Manser, W.S., Touati, M. and Barros, R.C., "The maximum sloshing wave height evaluation in cylindrical metallic tanks by numerical means", MATEC Web Conference., Vol. 95, (2017), 17005., https://doi.org/10.1051/matecconf/20179517005
5. Utsumi, M., "Vibration reduction of a floating roof by dynamic vibration absorbers", ***Journal of Pressure Vessel Technology***, Vol. 133, No. 4, (2011)., DOI: 10.1115/1.4002923
6. Kobayashi, N., Sato, T. and Torisaka, A., "Passive control of liquid sloshing in floating roof tank with multi dynamic absorber", in ASME 2013 Pressure Vessels and Piping Conference. Vol. Volume 8: Seismic Engineering, No. Issue, (2013)., DOI: 10.1115/pvp2013-97229
7. Hasheminejad, S.M. and Mohammadi, M.M., "Active sloshing control in a smart flexible cylindrical floating roof tank", ***Journal of Fluids and Structures***, Vol. 66, (2016), 350-381., https://doi.org/10.1016/j.jfluidstructs.2016.07.022
8. Esfandian, H., Goodarzian Urimi, M. and Shokoohi Rad, A., "Risk assessment of gasoline storage unit of national iranian oil product distribution company using phast software", ***International Journal of Engineering, Transactions A: Basics***, Vol. 34, No. 4, (2021), 763-768., DOI: 10.5829/IJE.2021.34.04A.02
9. Amabili, M., "Vibrations of circular plates resting on a sloshing liquid: Solution of the fully coupled problem", ***Journal of Sound and Vibration***, Vol. 245, No. 2, (2001), 261-283., https://doi.org/10.1006/jsvi.2000.3560
10. Golzar, F.G., Shabani, R., Tariverdilo, S. and Rezazadeh, G., "Sloshing response of floating roofed liquid storage tanks subjected to earthquakes of different types", ***Journal of Pressure Vessel Technology***, Vol. 134, No. 5, (2012)., DOI: 10.1115/1.4006858
11. Golzar, F.G., Shabani, R. and Tariverdilo, S., "Stress analyses in single deck and double deck floating roofs subjected to earthquake ground motions", ***Scientia Iranica***, Vol. 24, No. 2, (2017), 727-739., DOI: 10.24200/sci.2017.4057
12. Matsui, T., "Sloshing in a cylindrical liquid storage tank with a single-deck type floating roof under seismic excitation", ***Journal of Pressure Vessel Technology***, Vol. 131, No. 2, (2009)., DOI: 10.1115/1.3062939
13. Salarieh, H., shabani, r. and tariverdilo, s., "Effect of flexural and membrane stiffness on the analysis of floating roofs", ***International Journal of Engineering, Transactions A: Basics***, Vol. 23, No. 1, (2010), 57-64., http://www.ije.ir/article_71832_fcf49782751cad16e30f173312ef4676.pdf
14. Yamauchi, Y., Kamei, A., Zama, S. and Uchida, Y., "Seismic design of floating roof of oil storage tanks under liquid sloshing", in ASME 2006 Pressure Vessels and Piping/ICPVT-11 Conference. Vol. Volume 4: Fluid Structure Interaction, Parts A and B, (2006), 1407-1415., DOI: 10.1115/pvp2006-icpvt-11-93280
15. Sakai, F., Inoue, R. and Hayashi, S., "Fluid-elastic analysis and design of sloshing in floating-roof tanks subjected to earthquake motions", in ASME 2006 Pressure Vessels and Piping/ICPVT-11 Conference. Vol. Volume 4: Fluid Structure Interaction, Parts A and B, (2006), 1437-1446., DOI: 10.1115/pvp2006-icpvt-11-93622
16. Sakai F., I.R., "Some considerations on seismic design and controls of sloshing in floating-roofed oil tanks", in The 14th World Conference on Earthquake Engineering, Beijing, China. (2008).
17. Yoshida, S., Sekine, K. and Iwata, K., "Sloshing characteristics of single deck floating roofs in aboveground storage tanks: Natural periods and vibration modes", in ASME 2009 Pressure Vessels and Piping Conference. Vol. Volume 7: Operations, Applications and Components, (2009), 191-199., DOI: 10.1115/pvp2009-77187
18. Yoshida, S., Sekine, K. and Mitsuta, T., "Axisymmetric finite element analysis for sloshing response of floating roofs in cylindrical storage tanks", ***Journal of Environment and Engineering***, Vol. 5, No. 1, (2010), 27-38., DOI: 10.1299/jee.5.27

19. Utsumi, M., Ishida, K. and Hizume, M., "Internal resonance of a floating roof subjected to nonlinear sloshing", ***Journal of Applied Mechanics***, Vol. 77, No. 1, (2009)., DOI: 10.1115/1.3173768
20. Goudarzi, M.A., "Seismic behavior of a single deck floating roof due to second sloshing mode", ***Journal of Pressure Vessel Technology***, Vol. 135, No. 1, (2012)., DOI: 10.1115/1.4007291
21. Goudarzi, M.A., "Seismic design of a double deck floating roof type used for liquid storage tanks", ***Journal of Pressure Vessel Technology***, Vol. 137, No. 4, (2015)., DOI: 10.1115/1.4029111
22. Meera, U.S. and Reshmi, P.R., "Dynamic analysis of single deck floating roof with deck stiffeners", ***International Research Journal of Engineering and Technology***, Vol. 04, No. 04, (2017), 3522-3526., https://www.irjet.net/archives/V4/i4/IRJET-V4I4844.pdf
23. Hosseini, M., Soroor, A., Sardar, A. and Jafarieh, F., "A simplified method for seismic analysis of tanks with floating roof by using finite element method: Case study of kharg (southern iran) island tanks", ***Procedia Engineering***, Vol. 14, (2011), 2884-2890., https://doi.org/10.1016/j.proeng.2011.07.363
24. Belostotsky, A.M., Akimov, P.A. and Afansyeva, I.N., "Multilevel methodology of numerical seismic analysis of coupled systems "foundation – shell – pontoon (floating roof) – column(s) – fluid"", ***Procedia Engineering***, Vol. 153, (2016), 89-94., https://doi.org/10.1016/j.proeng.2016.08.085
25. Gnitko, V., Degtyariov, K., Naumenko, V. and Strelnikova, E., "Bem and fem analysis of the fluid-structure interaction in tanks with baffles", ***International Journal of Computational Methods and Experimental Measurements***, Vol. 5, No. 3, (2017), 317-328., DOI: 10.2495/CMEM-V5-N3-317-328
26. Shabani, R. and Golzar, F.G., "Large deflection analysis of floating roofs subjected to earthquake ground motions", ***Nonlinear Analysis: Real World Applications***, Vol. 13, No. 5, (2012), 2034-2048., https://doi.org/10.1016/j.nonrwa.2011.12.026
27. Sivy M., M.M., Chlebo O., Havelka R., "Sloshing effects in tanks containing liquid", in MATEC Web of Conferences, Bratislava, Slovakia. Vol. 107, (2017), 7., https://doi.org/10.1051/matecconf/201710700069
28. Shabani, R., "Stress patterns in single deck floating roofs subjected to ground motion accelerations", ***International Journal of Engineering, Transactions C: Aspects***, Vol. 26, No. 12, (2013), 1495-1504., DOI: 10.5829/idosi.ije.2013.26.12c.10
29. Yazdani, A.-. and Kowsari, M., "Statistical prediction of the sequence of large earthquakes in iran", ***International Journal of Engineering, Transactions B: Applications***, Vol. 24, No. 4, (2011), 325-336., DOI: 10.5829/idosi.ije.2011.24.04b.03
30. Chopra, A.K., "Dynamics of structures: Theory and applications to earthquake engineering", Fourth Edition ed, Berkeley, Prentice Hall, (2012)
31. ANSYS.Inc. *Customer support | ansys*. 26 August 2021]; Available from: https://www.ansys.com/support.,
32. NIOC, R.I.P.I. *Petroleum products specifications*. 26 August 2021]; Available from: https://www.nioc-intl.com/EN/PetroleumSpec.aspx
33. *Tank technology engineering service co. Ateco: External floating roof seals*. 26 August 2021]; Available from: https://www.atecotank.com/floating-roof-seal/external-floating-roof-seals/
34. Alzoubi, M., Al-Waked, R. and Tanbour, E., "Compression and hysteresis curves of nonlinear polyurethane foams under different densities, strain rates and different environmental conditions", ***Journal of Mechanical Engineering***, Vol. 9, (2011), 101-109., doi: 10.1115/IMECE2011-62290
35. Thomson, W.T. and Dahleh, M.D., "Theory of vibration with applications, India, Pearson, (1997), 544.
36. Moslemi, M. and Kianoush, M.R., "Parametric study on dynamic behavior of cylindrical ground-supported tanks", ***Engineering Structures***, Vol. 42, (2012), 214-230., https://doi.org/10.1016/j.engstruct.2012.04.026
37. Yenduri, A., Ghoshal, R. and Jaiman, R.K., "A new partitioned staggered scheme for flexible multibody interactions with strong inertial effects", ***Computer Methods in Applied Mechanics and Engineering***, Vol. 315, No., (2017), 316-347., https://doi.org/10.1016/j.cma.2016.10.044
38. Sivý, M. and Musil, M., "Seismic resistance of storage tanks containing liquid in accordance with principles of eurocode 8 standard", ***Strojnícky časopis - Journal of Mechanical Engineering***, Vol. 66, No. 2, (2016), 79-88., doi:10.1515/scjme-2016-0021
39. Norouzi, A.H., Gerami, M., Vahdani, R. and Sivandi-Pour, A., "Effects of multiple structure-soil-structure interactions considering the earthquake waveform and structures elevation effects", ***International Journal of Engineering, Transactions B: Applications***, Vol. 33, No. 5, (2020), 744-752., doi: 10.5829/ije.2020.33.05b.05
40. Seismosoft.Co. *Seismosignal support*. 26 August 2021]; Available from: https://seismosoft.com/support/seismosignal-support/
41. *Iran road, housing & urban development research center: Iran strong motion network*. 22 August 2021]; Available from: https://smd.bhrc.ac.ir/Portal/en/Search/BigQuakes
42. Standardization, E.C., *Eurocode 8- design of structures for earthquake resistance- part 4: Silos, tanks and pipelines*, in *Specific principles and application rules for tanks*. 2006, European Committee for Standardization: Brussels.81.

Persian Abstract

چکیده

ارتعاش لرزه‌ای سقف دوعرشه‌ای مخازن سیراف واقع در جنوب ایران بررسی گردیده است. میعانات گازی میدان نار و کنگان در جنوب ایران به عنوان هیدروکربن بسیارسبک، لاوان جهت نفت خام سبک و سروش برای نفت خام سنگین به عنوان محتویات مخزن در نظر گرفته شد. علاوه بر اندرکنش سیال–سازه، نقش آب‌بند فومی و اصطکاک تماسی بین آب‌بند و پوسته نیز مدنظر قرار گرفت. در شرایط ذکر شده فوق، تحلیل مودال و زمانی انجام شد. در تحلیل زمانی، زلزله‌های سرپل‌ذهاب و شنبه از استان زلزله‌ای زاگرس و ساکاریا از زلزله‌های مجاور ایران انتخاب گردید. فرکانس‌های طبیعی غالب، شکل‌مودهای اجزای سقف و ضریب میرایی فرکانس‌های طبیعی اول و دوم به همراه رفتار کلی زمانی و طیفی سقف برای هیدروکربن بسیار سبک تا سنگین ایران بدست آمده و ارزیابی شد. فرکانس طبیعی هیدروالاستیک سقف در نفت سروش حدود ۱۷٪ و ضریب میرایی حدود ۱۰٪ نسبت به حالت میعانات گازی کاهش داشت. محاسبات نشان داد فرکانس‌های طبیعی هیدروالاستیک غالب و ضرایب میرایی آنها با سنگین شدن مایع کاهش می‌یابد و ارتعاش سقف اساسا" به رابطه محتویات فرکانسی زلزله با این فرکانس‌های طبیعی بستگی دارد. همچنین نتیجه‌گیری شد بر اساس روش مقیاس و دامنه ارتعاش حالت پایدار، سقف شناور در حالت مایع سنگین‌تر لرزه‌پذیری بیشتری دارد.